

Inertial focusing of slightly non-neutrally buoyant finite-size particles in microchannels

By Alexander L. Dubov¹, Tatiana V. Nizkaya¹, Jens Harting^{2,3,4}, Olga I. Vinogradova^{1,5,6} and Evgeny S. Asmolov^{1,7} †

¹A.N. Frumkin Institute of Physical Chemistry and Electrochemistry,

Russian Academy of Sciences, 31 Leninsky Prospect, 119071 Moscow, Russia

²Helmholtz Institute Erlangen-Nürnberg for Renewable Energy, Forschungszentrum Jülich, Fürther Str. 248, 90429 Nürnberg, Germany

³Department of Applied Physics, Eindhoven University of Technology, PO box 513, 5600MB Eindhoven, The Netherlands

⁴ Faculty of Science and Technology, University of Twente, 7500 AE Enschede, The Netherlands

⁵Department of Physics, M. V. Lomonosov Moscow State University, 119991 Moscow, Russia

⁶DWI - Leibniz Institute for Interactive Materials, Forckenbeckstr. 50, 52056 Aachen, Germany

⁷Institute of Mechanics, M. V. Lomonosov Moscow State University, 119991 Moscow, Russia

(Received Received: date / Accepted: date)

The migration of spherical particles of different sizes and buoyancies in channels has an impact on the transport of suspensions and for applications in inertial microfluidics. At intermediate Reynolds numbers, both, inertial lift and gravity contribute to particle migration in horizontal or inclined channels. By means of lattice Boltzmann simulations we study the role of a slip velocity which is due to hydrodynamic interactions with walls or due to the effect of gravity. The slip velocity of a neutrally buoyant particle is finite in near-wall regions, and its effect on the lift is significant in close proximity of the walls. We propose a simple formula for the lift coefficient which combines theoretical predictions for point particles in a channel flow (Vasseur & Cox 1976) and for finite-size particles in a wall-bounded simple linear flow (Cherukat & McLaughlin 1994). Particle equilibrium positions of non-neutrally buoyant particles are defined by the balance of the two forces and are shifted into near-wall regions. The contributions of the shear-induced and the gravity-induced slip velocities to the lift are additive. This fact can be used to predict equilibrium positions of non-neutrally buoyant particles in inclined channels.

1. Introduction

The rapid development of inertial microfluidics led to an increased interest in the lift on finite-size particles in confined flows (Di Carlo *et al.* 2007; Bhagat *et al.* 2008). It is well known that neutrally buoyant particles in a channel focus to some equilibrium positions where the lift vanishes (Segré & Silberberg 1962). Inertial focusing has become a basis for various methods of particle separation by size or by shape (see Martel & Toner (2014) and Zhang *et al.* (2016) for recent reviews). In these applications the lift is equilibrated with the drag originating from an auxiliary flow, such as a Dean vortex in a curved channel (Bhagat *et al.* 2008). This leads to changed equilibrium positions for different particles. The same effect could be obtained by balancing the lift and some external force, e.g. electric (Zhang *et al.* 2014), magnetic (Dutz *et al.*

† Author to whom correspondence should be addressed; email: aes50@yandex.ru

2017) or gravitational. Alternatively, the particle deformability has a strong impact on inertial focusing and particle structuring in channel flows (Krüger *et al.* 2014).

The equilibrium positions of neutrally-buoyant particles in channel flow have been studied experimentally (Matas *et al.* 2004; Miura *et al.* 2014; Hood *et al.* 2016; Morita *et al.* 2017), numerically (Di Carlo *et al.* 2009; Liu *et al.* 2015; Loisel *et al.* 2015), and by computer simulations (Chun & Ladd 2006; Kilimnik *et al.* 2011). Several power laws have been proposed (Di Carlo *et al.* 2009; Hood *et al.* 2015; Liu *et al.* 2016) for the lift in the central and in the near-wall regions of the channel.

An asymptotic approach (Ho & Leal 1974; Vasseur & Cox 1976; Cox & Hsu 1977; Schonberg & Hinch 1989; Cherukat & Mclaughlin 1994; Asmolov 1999; Matas *et al.* 2004, 2009) is applied for spherical particles at small Reynolds number $\text{Re}_p = a^2 G/\nu$, where a is the particle radius, G is the characteristic shear rate and ν is the kinematic viscosity. To the leading order in Re_p , the disturbance flow is governed by the Stokes equations, and a spherical particle experiences a drag and a torque but no lift. The lift is deduced from the solution of the next-order equations which involve small advective (fluid-inertia) terms and thus accounts a non-linear coupling between the shear background and disturbance flows. The Stokeslet disturbance originates from a particle translational motion relative to the carrier fluid, and the stresslet is generated by the rotation of the sphere in the shear flow. The lift also includes the contributions due to the two disturbances (Vasseur & Cox 1976),

$$F_l^i = \rho a^2 (c_{10} a^2 G^2 + c_{11} a G V_s^i + c_{12} V_s^{i2}), \quad (1.1)$$

where ρ is the fluid density, $V_s^i = V^i - U^i$ and V^i are the particle slip and translational velocities and U^i is the velocity of the undisturbed flow at the sphere center. Hereafter we use primed variables to denote dimensional forces and velocities. The first term in (1.1) originates from the particle rotation in shear flow, the second term corresponds to a coupling between the particle rotational and translational motion and the third term is purely translational. The coefficients c_{1i} ($i = 0, 1, 2$) generally depend on many dimensionless groups: z/a , H/a , V^i/U_m^i and channel Reynolds number $\text{Re}_{ch} = U_m^i H/\nu$, where z is the distance to the closest wall, H is the channel width and U_m^i is the maximum velocity of the channel flow.

The slip velocity may arise under an external force, e.g., gravity for non-neutrally buoyant particles, and this contribution to the lift dominates when $V_s^i \gg Ga$. For neutrally buoyant particles, it is believed (Ho & Leal 1974; Hood *et al.* 2015) that the slip velocity is negligible, and the lift is due to the stresslet only. This is true for small particles far from walls, $a/z \ll 1$, but hydrodynamic interactions at finite distances $z \sim a$ induce a finite slip, $V_s^i \sim Ga$, and all contributions to the lift become comparable. Asymptotic solutions for finite-size particles have been obtained for shear flows near an isolated wall only (Cherukat & Mclaughlin 1994; Yahiaoui & Feuillebois 2010). However, it remains unclear how these results can be applied to the channel flow.

In this paper we consider the migration of finite-size particles at moderate channel Reynolds numbers, $\text{Re}_{ch} \sim 10$. The effect of the slip velocity on the lift for both, neutrally and non-neutrally buoyant particles is studied. We propose a hybrid formula for the lift on a neutrally buoyant particle which combines the theoretical results for point (Vasseur & Cox 1976) and finite-size particles (Cherukat & Mclaughlin 1994). We use the lattice Boltzmann method to simulate particle motion, to measure the migration and the slip velocities, and to check the validity of the formula. Finally, we simulate some trajectories for particles with a small density contrast and show that such particles can be efficiently separated within the near-wall region.

2. Theory

The system studied is depicted in figure 1. A spherical particle of radius a translates in a pressure-driven flow confined by two parallel flat walls, separated by a distance H . The undis-

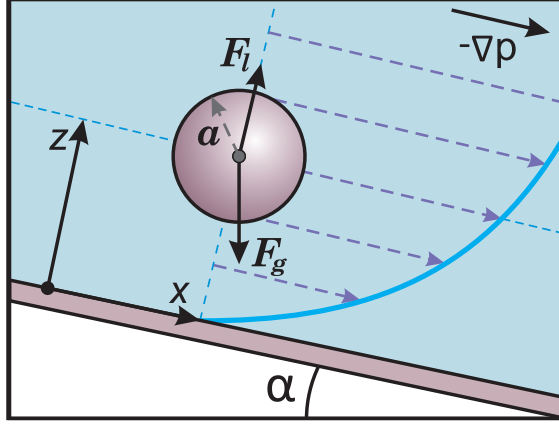


FIGURE 1. Sketch of particle migration in a pressure-driven flow.

turbed velocity profile is

$$U'(z) = 4U'_m z(1 - z/H)/H. \quad (2.1)$$

We consider both, neutrally buoyant (the particle density ρ_p is equal to the fluid density ρ) and slightly non-neutrally buoyant particles assuming that $V'_s \sim G_m a$, where $G_m = 4U'_m/H$ is the maximum shear rate at the channel wall. The channel can be inclined (an inclination angle $\alpha = 0$ corresponds to a horizontal channel), when the gravity force has components streamwise and normal to the walls. The lift (1.1) can be written in the form

$$F'_l = \rho a^4 G_m^2 c_l, \quad (2.2)$$

$$c_l = c_{l0} + c_{l1} V_s + c_{l2} V_s^2, \quad (2.3)$$

where c_l is the lift coefficient and $V_s = V'_s/(aG_m)$ is a dimensionless slip velocity.

Asymptotic theories provide solutions for c_l in some limiting cases only, but there is no equation for finite particles being uniformly valid over the entire channel width. Vasseur & Cox (1976) have applied the point-particle approximation to obtain the coefficients $c_{l0}^{VC}, c_{l1}^{VC}, c_{l2}^{VC}$ at small channel Reynolds numbers and $z \gg a$ which depend on z/H only. Cherukat & McLaughlin (1994) have evaluated the coefficients $c_{li}^{CM}(z/a)$, $i = 0, 1, 2$ for the finite-sized particle ($z \sim a$) in a wall-bounded linear shear flow and proposed simple fits for them (see Appendix A). The dependencies for quadratic flow $c_{li}(z/a, H/a)$ (Yahiaoui & Feuillebois 2010) are too complicated, and the effect of the second wall cannot be accounted correctly.

2.1. Neutrally buoyant particles

The slip velocity of a freely rotating particle has been found theoretically for a wall-bounded linear shear flow by Goldman *et al.* (1967) and for a quadratic flow by Pasol *et al.* (2006). It decays rapidly with the distance from the wall, like $(a/z)^3$ (Wakiya *et al.* 1967). Therefore, the slip contribution to the lift can be neglected when $a/z \ll 1$. Such a particle is equivalent to a dipole. For small gaps between the sphere and the wall, there is an expansion for the slip velocity (Goldman *et al.* 1967):

$$V_s = -1 + \frac{0.7431}{0.6376 - 0.200 \log(z/a - 1)} \quad \text{at } z/a - 1 \ll 1. \quad (2.4)$$

A logarithmic singularity in (2.4) means that the lift coefficient (2.3) cannot be fitted by any power law $(a/z)^n$ in the near-wall region. The slip and stresslet contributions are comparable when $z \sim a$. The limiting values following from the two approaches differ significantly: $c_l =$

$c_{l0}^{CV}(0) = 55\pi/96 \simeq 1.8$ for the dipole close to the wall ($a \ll z \ll H$) (Cox & Hsu 1977), and $c_l^{CM}(1) = 9.28$ which is close to the coefficient $c_l^{KL} = 9.257$ (Krishnan & Leighton Jr. 1995) for a particle being in contact with the wall.

Thus, the first term in (2.3) (stresslet contribution) is finite for any z , while the second and the third ones (Stokeslet contribution) are finite for $z \sim a$ only. The coefficient $c_{l0}^{CM}(z/a)$ is nearly constant (see Cherukat & McLaughlin 1994, figure 5) and tends to the limiting value $c_{l0}^{VC}(0)$ as $z \gg a$. This enables us to construct the following hybrid formula for the lift coefficient:

$$c_{l0} = c_{l0}^{VC}(z/H) + \gamma c_{l1}^{CM}(z/a)V_s + c_{l2}^{CM}(z/a)V_s^2, \quad (2.5)$$

where $\gamma = G(z)/G_m = 1 - 2z/H \leq 1$ is a dimensionless local shear rate at the particle position. This correction factor takes into account the variation of G in the second term of Eq. (1.1) and ensures the lift to remain zero at the channel centerline. We neglect the effects due to quadratic flow and due to the second wall (corrections of order a/H) in the second and in the third term in Eq. (2.5). The formula proposed is asymptotically valid for any z when $a/H \ll 1$ and $\text{Re}_{ch} \ll 1$. Our simulations (Sec. 4.1) show that it provides a proper accuracy for $a/H \leq 0.1$ and moderate Reynolds numbers $\text{Re}_{ch} \leq 22.5$.

2.2. Non-neutrally buoyant particles

There is an additional force for non-neutrally buoyant particles that results from imbalance between gravity and buoyancy. The dimensionless value is introduced in the same way as the lift,

$$F_g = \frac{F'_g}{\rho a^4 G_m^2} = \frac{4\pi g}{3aG_m^2} \Delta\rho, \quad (2.6)$$

where $\Delta\rho = (\rho_p - \rho)/\rho$ is the density contrast. Particle equilibrium positions in a horizontal channel z_{eq} can be deduced from the balance between the lift and the gravity,

$$c_l(z_{eq}) = F_g. \quad (2.7)$$

The equation may have two, one or no stable equilibrium points which depends on the parameter F_g only. The sensitivity of equilibrium positions to the particle size or to the density contrast is defined by the value $\partial c_l / \partial z$. When the derivative is small, small variations in F_g lead to a significant shift in focusing positions. The range of possible z_{eq} can be tuned by the choice of G_m .

Particles in inclined channels have an additional slip velocity due to gravity. It is equal to the Stokes velocity, $V'_s = F'_g \sin \alpha / (6\pi\mu a)$ where μ is the dynamic viscosity, for small particles far from the walls. When $z \sim a$ the drag coefficient in the channel changes due to hydrodynamic interactions with the walls, and no simple expression is available for V'_s . However, the general form (2.3) is still valid and the contribution of the gravity-induced slip velocity to the lift can be extracted from simulation data.

3. Simulation method

The lattice Boltzmann method (Benzi *et al.* 1992; Kunert *et al.* 2010; Dubov *et al.* 2014) is used to simulate particle motion in channel flow. The simulation cell is bounded by two walls with no-slip boundary conditions at $z = 0$ and $z = 79\delta$ and two periodic boundaries with $N_x = N_y = 256\delta$, where δ is the lattice spacing. Spherical particles of radii $a = 4\delta - 12\delta$ are implemented as moving no-slip boundaries (Ladd & Verberg 2001; Janoschek *et al.* 2010; Harting *et al.* 2014). By applying a body force which is equivalent to a pressure gradient $-\nabla p$ a Poiseuille flow is obtained. We use a 3D, 19 velocity, single relaxation time implementation of the lattice Boltzmann method, where the relaxation time τ is kept to 1 throughout this paper. Different flow rates are obtained by changing the fluid forcing. We use two channel Reynolds numbers $\text{Re}_{ch} = 11.3$

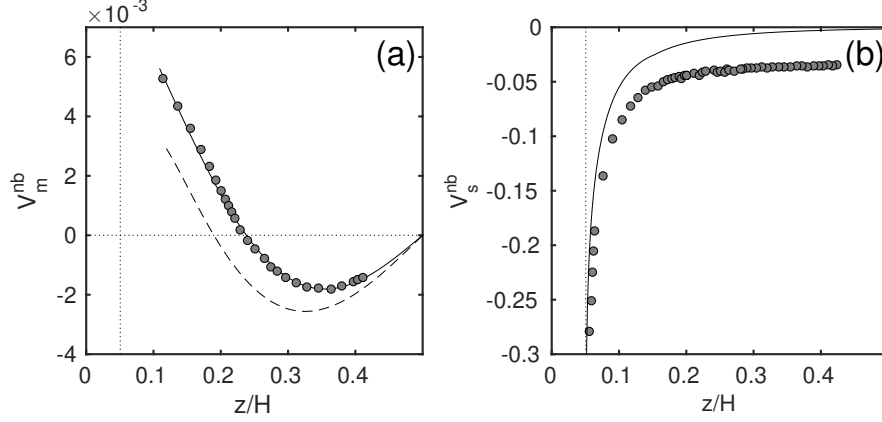


FIGURE 2. Dimensionless (a) migration and (b) slip velocities as functions of particle position z/H for particles with $a = 4\delta$. Only a half of the channel since the curves are antisymmetric with respect to the channel axis $z = H/2$. Symbols are the simulation results. The dashed line in (a) is the prediction of the point-particle theory (Vasseur & Cox 1976), while the solid line in (b) is the slip velocity in a wall-bounded linear shear flow (Goldman *et al.* 1967). Vertical dotted lines correspond to the particle contact with the wall.

and $Re_{ch} = 22.6$ in the simulations to verify whether the lift coefficient depends on Re_{ch} . The gravity force is applied to the center of the particle and directed at an angle α relative to the z -axis to simulate the migration in an inclined channel. The dimensionless value F_g varies from 0 (neutrally buoyant particle) to 13.91.

We measure the x - and z -components of the particle velocity in our computer experiments, and find the dimensionless slip-, $V_s = (V'_x - U'(z))/(aG_m)$, and migration velocities, $V_m = V'_z/(aG_m)$. The lift can be extracted from these calculations, assuming that the particle motion is quasi-stationary. The lift is balanced by the z - component of the drag, $F'_l = -F'_{dz}$. Following Dubov *et al.* (2014), the drag between parallel walls is given by

$$F'_{dz} \approx -6\pi\mu a V'_m f_z(z/H, a/H), \quad (3.1)$$

$$f_z = 1 + \frac{a}{z-a} + \frac{a}{H-a-z}. \quad (3.2)$$

The second and the third term in (3.2) are corrections to the Stokes drag due to hydrodynamic interactions with the two walls.

Another method used to calculate the lift and to check the validity of the first approach is to balance the lift by the gravity force on a non-neutrally buoyant particle in a horizontal channel (see (2.7) and Sec. 4.2). By changing the gravity force F_g one can span the whole range of equilibrium positions within the channel and recover the full $c_l(z)$ curve. The advantage of this method is that it does not require the particle motion to be quasi-stationary. The drawback is that the convergence to equilibrium can be slow in central zones of the channel, where the slope of $c_l(z)$ is small. We extract the lift from the migration velocity using (3.1), (3.2) throughout the channel and additionally verify the results in the near-wall region by equilibration (2.7).

4. Results and discussion

4.1. Neutrally buoyant particles

The migration V_m^{nb} and the slip V_s^{nb} velocities of the neutrally buoyant particle with $a = 4\delta$ are presented in figure 2 as functions of particle position z/H (we show only a half of the channel since the curves are antisymmetric with respect to the channel axis $z = H/2$). The simulated

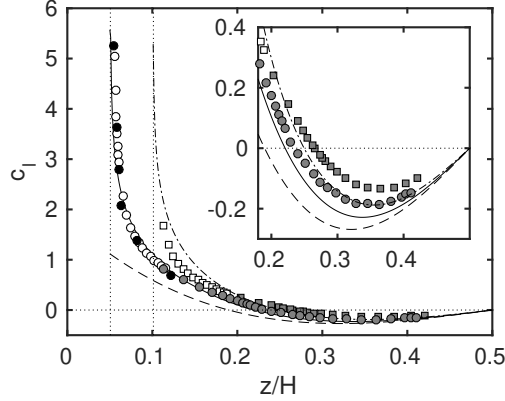


FIGURE 3. Lift coefficient c_l for neutrally buoyant particles evaluated from the data for the migration velocity at $\text{Re}_{ch} = 11.3$ (grey symbols) and $\text{Re}_{ch} = 22.6$ (white symbols) and from the force balance of non-neutrally buoyant particles in the horizontal channel at $\text{Re}_{ch} = 22.6$ (black symbols). Circles correspond to $a = 4\delta$ and squares to $a = 8\delta$. Solid and dash-dotted lines are Eqs. (2.5), (A 2)-(A 5), (A 7)-(A 11) for $a = 4\delta$ and $a = 8\delta$, respectively. Vertical dotted lines correspond to the particle contact with the wall and the dashed line is the prediction of the point-particle theory (Vasseur & Cox 1976). The inset depicts the lift coefficient in the central channel part.

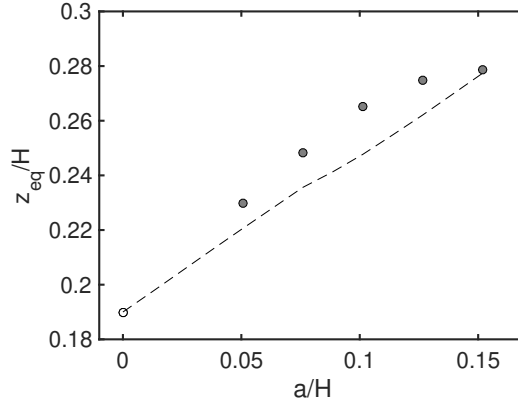


FIGURE 4. Equilibrium positions for finite-sized neutrally buoyant particles (grey circles). The dashed line is estimated using Eq. (2.5) and the white circle corresponds to the prediction for point particles (Vasseur & Cox 1976).

migration velocity differs significantly from the velocity $c_{l0}\text{Re}_p/(6\pi)$, where $\text{Re}_p = a^2 G_m/\nu$, as follows from the point-particle theory (Vasseur & Cox 1976). As the particle approaches the wall, this deviation grows. The equilibrium position where $V_m^{nb} = 0$ is shifted towards the channel axis. This effect is due to particle interactions with the wall resulting in a finite slip velocity. Indeed, we can see in figure 2(b) that the measured V_s^{nb} grows rapidly near the wall and is close to the theoretical predictions for a linear shear flow near a single wall (Goldman *et al.* 1967). Unlike proposed by the theoretical values, the residual slip velocity is non-zero in the central part of the channel. We expect this to be due to the Faxen correction to the slip and due to hydrodynamic interactions with the walls in a quadratic flow.

The lift coefficient is extracted from the data for the migration velocity using (2.2) and (3.1) and is presented in figure 3. The results are shown for $\text{Re}_{ch} = 11.3$ and $\text{Re}_{ch} = 22.6$, $a = 4\delta$ and 8δ . They are close for the two Reynolds numbers, thus supporting the prediction that the lift

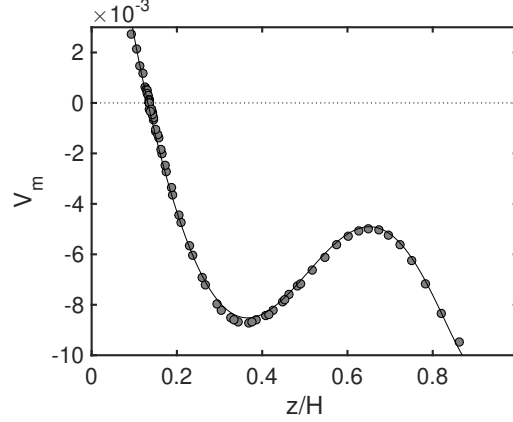


FIGURE 5. Migration velocity for the non-neutrally buoyant particle in the horizontal channel. Symbols correspond to simulation data and the solid line is calculated using (4.1) and data for a neutrally buoyant particle.

does not depend on Re_{ch} up to 20. Our hybrid formula (2.5) provides a very good agreement for smaller particles with $a = 4\delta$, especially in the near-wall zone, where the point-particle theory of Vasseur & Cox (1976) (dashed line) fails. The discrepancy between the fit and the simulation data is more pronounced for bigger particles, but still much smaller than that for the point-particle theory. It is due to the effects of quadratic flow (of order $O(a/H)$) in evaluating the slip velocity and the stresslet (see Yahiaoui & Feuillebois 2010; Hood *et al.* 2015). The deviation is also greater near the equilibrium positions and in the central part of the channel.

The equilibrium position depends almost linearly on the particle size for a/H up to 0.1 (see figure 4). The trend of the numerical results coincides with the theoretical limit $z_{eq}/H \simeq 0.19$ for $a \ll H$. The formula adequately predicts the shift of equilibrium positions towards the channel center but with a slightly smaller slope of the curve.

4.2. Non-neutrally buoyant particles

We now move to particle migration under inertial lift and gravity. We show that the general additive form of (2.3) is still valid in this case. Also, these calculations enable us to check the results obtained for neutrally buoyant particles with the use of (3.1).

We first consider a horizontal channel where the gravity force is perpendicular to the channel walls. The simulation data for the migration velocity of a particle with radius $a = 4\delta$ and dimensionless gravity force $F_g = 0.694$ is presented in figure 5. The solid curve denotes the migration velocity calculated directly by fitting the data V_m^{nb} for neutrally-buoyant particles (figure 2(a)):

$$V_m = V_m^{nb} - V^{St}/f_z, \quad (4.1)$$

where $V^{St} = \text{Re}_p F_g / (6\pi)$ is the dimensionless Stokes settling velocity. The agreement is perfect, and this confirms the validity of the approximation (3.1)–(3.2) for the z -component of the drag force. The particle migrates towards a single equilibrium position where $c_l = F_g$. Therefore, such simulations also enable us to find the exact values of the lift coefficient for different z by varying F_g and thus to recover the $c_l(z)$ curve. The results obtained in this way are shown by black symbols in figure 3 and compare very well with the other data.

We also simulate particle motion in vertical channels (the gravity force is parallel to the flow direction). The slip and the migration velocities are presented in figures 6(a) and 7(a), respectively for several values of F_g . The linearity of the Stokes equations governing disturbance flow at small particle Reynolds numbers enables us to decompose the particle slip velocity into two

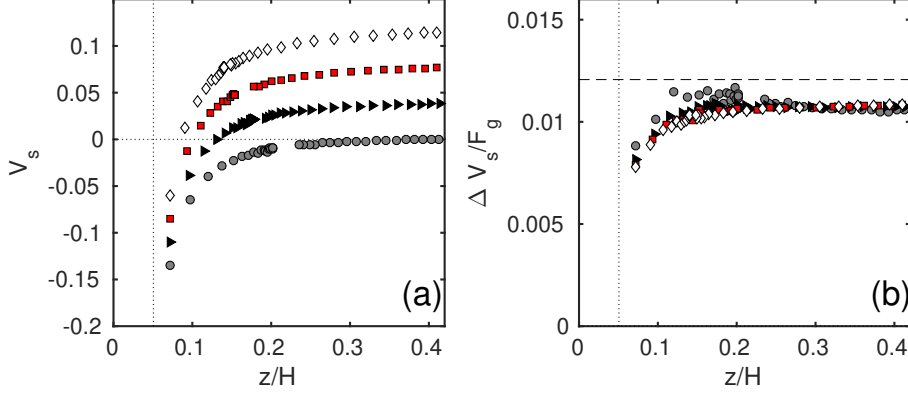


FIGURE 6. (a) Slip velocities for non-neutrally buoyant particles with $a = 4\delta$ and different gravity forces, $F_g = 3.475$ (gray circles), 6.956 (black triangles), 10.44 (red squares) and 13.91 (white diamonds) in a vertical channel. (b) Rescaled difference of slip velocities for non-neutrally and neutrally buoyant particles. The dashed line depicts V^{St} . Vertical dotted lines correspond to the particle contact with the wall.

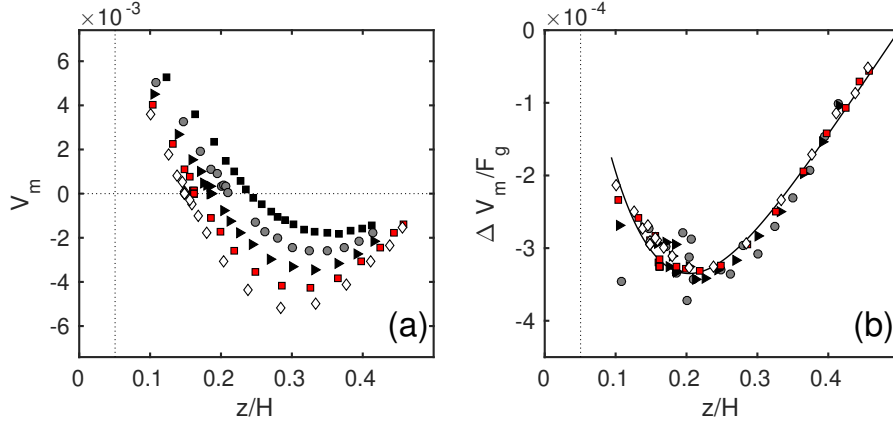


FIGURE 7. (a) Migration velocities in a vertical channel. (b) Rescaled difference of migration velocities for non-neutrally and neutrally buoyant particles $\Delta V_m / F_g$. Vertical dotted lines correspond to the particle contact with the wall, black squares in (a) to neutrally buoyant particles. For further details see the caption of figure 6.

contributions due to the particle-wall interaction and to the gravity force,

$$V_s = V_s^{nb} - V^{St} / f_x, \quad (4.2)$$

where $f_x(z/H, a/H)$ is the correction to the drag for a particle translating parallel to the channel walls. We calculate $\Delta V_s = V_s - V_s^{nb}$ from the numerical data of figures 2(a) and 6(a). The results are shown in figure 6(b) and collapse onto a single curve, thus confirming (4.2). The rescaled slip-velocity difference is nearly constant in the central zone, remaining slightly less than V^{St} due to the influence of channel walls. The deviation grows close to the wall.

The change in the slip velocity due to gravity is small for slightly non-neutrally buoyant particles (see figure 6). In this case equation (2.5) can be linearized with respect to ΔV_s :

$$c_l \simeq c_l^{nb} + \Delta V_s (c_{l1}^{CM} + 2c_{l2}^{CM} V_s^{nb}), \quad (4.3)$$

where $c_l^{nb} = c_l(V_s^{nb})$ is the lift coefficient for neutrally buoyant particles. We evaluate $\Delta V_m / F_g =$

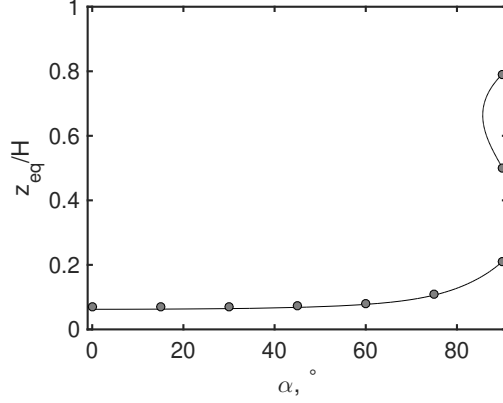


FIGURE 8. Equilibrium positions z_{eq}/H for $a = 4\delta$ and $F_g = 3.475$. Circles are simulation data, the line is the prediction of (4.4).

$(V_m - V_m^{nb})/F_g$ from the numerical data in figures 2 and 7(a). The results are presented in figure 7(b) and also collapse onto a single curve, which confirms the linearization (4.3).

For an arbitrary inclination angle α of the channel, the z -component of the force reads

$$F_z = c_l(V_s) + F_g \cos \alpha, \quad (4.4)$$

$$V_s = V_s^{nb} - V^{St} \sin \alpha / f_x, \quad (4.5)$$

where c_l is calculated using (4.3). Figure 8 shows particle equilibrium positions as a function of α . The values calculated using (4.4), (4.5) and the fit curve from figure 7(b) compare very well with the simulation data. There are three equilibrium positions for the nearly vertical channel, $\alpha > 85.7^\circ$. Two positions near the walls are stable and the one in the middle of the channel is unstable. For smaller α and given F_g we have only one equilibrium position which is sensible to the inclination angle for $\alpha > 60^\circ$.

4.3. Separation of particles in a horizontal channel

The results obtained in the previous subsections for moderate Reynolds numbers, $Re_{ch} < 20$, can be applied at smaller values, since the lift coefficient is independent of Re_{ch} . In this case the gravity force and the inertial lift may be of the same order even at small density contrast $\Delta\rho$. The equilibrium positions z_{eq} strongly depend on F_g (see figure 9(a)), and this can be utilized to separate slightly non-neutrally buoyant particles by the value $\Delta\rho$.

Simulations of migration at small Re_{ch} require a very long migration time, $v / (G_m a)^2 = (4G_m Re_{ch})^{-1} (H/a)^2$ (see Appendix B). This difficulty can be overcome if one introduces dimensionless coordinates $\zeta = z/a$, $\xi = xG_m a/v$. Particle trajectories written in terms of ζ , ξ are also independent of Re_{ch} , so simulation results obtained at moderate Reynolds number can be used at smaller Re_{ch} .

To illustrate the effect of F_g we show in figure 9(b) several simulated trajectories of particles injected close to the bottom wall in a horizontal channel at $Re_{ch} = 11.3$. When F_g is high the particle drops to the wall (lowest trajectory). The other particles follow divergent trajectories leading to their respective equilibrium positions. The channel Reynolds number can be chosen so that a small variation in particle density provides a noticeable difference in F_g and thus enables separation. For example, if we use the parameters $Re_{ch} = 0.3$, $a = 2 \mu\text{m}$ and $H = 40 \mu\text{m}$, typical for a microfluidic experiment, the four trajectories shown in figure 9 (from top to bottom) correspond to small density differences: $\Delta\rho/\rho = 0.007, 0.022, 0.037$ and 0.073 . The length of the region (the channel length) shown in the figure is $L_{ch} \simeq 3.3 \text{ cm}$. Indeed, trajectories of particles

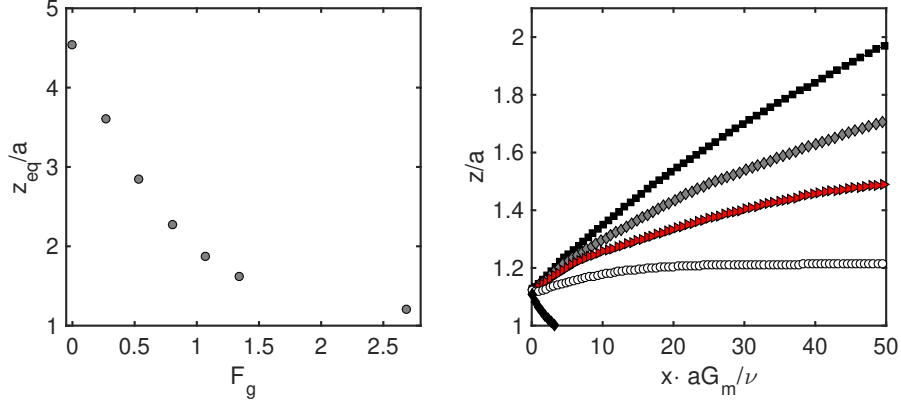


FIGURE 9. (a) Equilibrium positions of non-neutrally buoyant particles with $a = 4\delta$ in a horizontal channel; (b) trajectories of particles with $a = 4\delta$ and different $F_g = 0.268$ (black squares), 0.804 (grey diamonds), 1.340 (red triangles), 2.681 (open circles), 9.383 (black diamonds), released at $z_0 = 1.125a$.

with different F_g diverge, especially when they start in the near-wall region where the lift varies significantly with the distance from the wall.

We have shown in a recent experimental work (Asmolov *et al.* 2015) that particles translating in a channel with the bottom wall decorated by a superhydrophobic texture can be shifted in a transverse direction. The effect is due to a secondary transverse flow induced by the anisotropic pattern and depends on the particle distance to the wall. So it can be used in combination with the inertial migration to separate particles with different a or F_g not only by vertical but also by their transverse positions.

5. Conclusions

We have studied inertial migration of neutrally and non-neutrally buoyant finite-size particles in a channel flow using lattice-Boltzmann simulations. We have highlighted the importance of the particle slip velocity, which is non-zero even for neutrally buoyant particles due to the hydrodynamic interactions with channel walls. We have proposed a hybrid formula for the lift which combines asymptotic theories for finite-size particles near a single wall and for point particles in the channel. The formula provides a proper agreement with the simulation data for particles of small but finite size $a/H < 0.1$, especially in the near-wall region. The equilibrium positions for heavy particles can be predicted using the data for the neutrally-buoyant case. For particles in inclined channels, gravity induces an additional slip velocity contributing to the lift. Our simulation results confirm the additive form of the lift in this case. Finally, we show that channel flows with small Reynolds numbers $Re_{ch} \sim 1$ can be used for the separation of particles with small density contrast.

We thank Sebastian Schmieschek and Manuel Zellhöfer for their help on technical aspects of the simulations. This research was partly supported by the Russian Foundation for Basic Research (grant 15-01-03069).

Appendix A. Fits for the slip velocity and the lift coefficients

In this Appendix we summarize known results for the slip velocity and the lift coefficients for finite-size particles in a linear shear flow near a single wall and for point particles in Poiseuille flow. The velocity of a freely translating and rotating particle in a linear shear flow is given by (Goldman *et al.* 1967)

$$V'_x = U'(z)h(z/a). \quad (\text{A } 1)$$

We use (A 1) to estimate the slip velocity in channel flow, i.e., we neglect the effects due to quadratic flow, so that

$$V_s = \frac{z(H-z)(h-1)}{aH}. \quad (\text{A } 2)$$

The correction factor fitting the results by Goldman *et al.* (1967) in the near-wall region reads (Reschiglian *et al.* 2000)

$$h = \frac{200.9b - (115.7b + 721)\zeta^{-1} - 781.1}{-27.25b^2 + 398.4b - 1182} \quad \text{at } \zeta < 3, \quad (\text{A } 3)$$

$$\zeta = \frac{z}{a}, \quad b = \log(\zeta - 1). \quad (\text{A } 4)$$

Here, we have rewritten the equation from the original paper (Reschiglian *et al.* 2000) in terms of the natural logarithm. For greater distances we use the asymptotic solution by Wakiya *et al.* (1967),

$$h = \frac{1 - \frac{5}{4}\zeta^{-3} + \frac{5}{4}\zeta^{-5} - \frac{23}{48}\zeta^{-7} - \frac{1375}{1024}\zeta^{-8}}{1 - \frac{15}{16}\zeta^{-3} + \zeta^{-5} - \frac{3}{8}\zeta^{-7} - \frac{4565}{4096}\zeta^{-8}} \quad \text{at } \zeta \geq 3. \quad (\text{A } 5)$$

Vasseur & Cox (1976) have obtained the lift on a small particle in channel flow at $z \gg a$ and $\text{Re}_{ch} \ll 1$ using a point-particle approximation:

$$c_l^{VC} = c_{l0}^{VC} + \frac{H}{a}c_{l1}^{VC}V_s + c_{l2}^{VC}V_s^2. \quad (\text{A } 6)$$

The coefficients $c_{l0}^{VC}, c_{l1}^{VC}, c_{l2}^{VC}$ depend on z/H only. The following simple fit to the first term has been proposed by Feuillebois (2004):

$$c_{l0}^{VC} = 2.25(z/H - 0.5) - 23.4(z/H - 0.5)^3. \quad (\text{A } 7)$$

The lift coefficient for a finite-size particle in a linear shear flow bounded by a single wall is (Cherukat & Mclaughlin 1994)

$$c_l^{CM} = c_{l0}^{CM} + c_{l1}^{CM}V_s + c_{l2}^{CM}V_s^2, \quad (\text{A } 8)$$

where the coefficients $c_{l0}^{CM}, c_{l1}^{CM}, c_{l2}^{CM}$ depend on $\zeta = z/a$ only,

$$c_{l0}^{CM} = 1.8081 + 0.879585\zeta^{-1} - 1.9009\zeta^{-2} + 0.98149\zeta^{-3}, \quad (\text{A } 9)$$

$$c_{l1}^{CM} = -3.24139\zeta - 2.676 - 0.8248\zeta^{-1} + 0.4616\zeta^{-2}, \quad (\text{A } 10)$$

$$c_{l2}^{CM} = 1.7631 + 0.3561\zeta^{-1} - 1.1837\zeta^{-2} + 0.845163\zeta^{-3}. \quad (\text{A } 11)$$

Appendix B. Particle trajectories

The components of the particle velocity can be written as

$$\frac{dx}{dt} = V'_x = U'(z)h = G_m z(1 - z/H)h, \quad (\text{B } 1)$$

$$\frac{dz}{dt} = V'_m = \frac{F'_l - F'_g}{6\pi\mu a f_z} = \frac{(c_l - F_g) a^3 G_m^2}{6\pi\nu f_z}. \quad (\text{B } 2)$$

The last equation means that the migration time, i.e., the time required to migrate at distance of order a , is $\nu / (G_m a)^2 = (4G_m \text{Re}_{ch})^{-1} (H/a)^2$.

Since the right-hand sides of (B 1) and (B 2) do not involve the time explicitly, we can write the equation governing the particle trajectory as

$$\frac{dz}{dx} = \frac{a^3 G_m}{6\pi\nu} \frac{c_l - F_g}{f_z z (1 - z/H) h}.$$

We introduce dimensionless coordinates by

$$\zeta = z/a, \quad \xi = xG_m a/\nu, \quad (\text{B } 3)$$

to obtain

$$\frac{d\zeta}{d\xi} = \frac{1}{6\pi} \frac{c_l - F_g}{f_z h \zeta (1 - \zeta a/H)}. \quad (\text{B } 4)$$

The lift coefficient exhibits only a weak dependence on the Reynolds number for moderate Re_{ch} , while the other dimensionless functions are all independent of Re_{ch} . Hence, we can use the last equation to model particle motion for the same F_g and a/H but for different Re_{ch} .

REFERENCES

- ASMOLOV, E. S. 1999 The inertial lift on a spherical particle in a plane Poiseuille flow at large channel Reynolds number. *J. Fluid Mech.* **381**, 63–87.
- ASMOLOV, E. S., DUBOV, A. L., NIZKAYA, T. V., KUEHNE, A. J. C. & VINOGRADOVA, O. I. 2015 Principles of transverse flow fractionation of microparticles in superhydrophobic channels. *Lab. Chip* **15** (13), 2835–2841.
- BENZI, R., SUCCI, S. & VERGASSOLA, M. 1992 The lattice Boltzmann equation: theory and applications. *Physics Reports* **222**, 145.
- BHAGAT, A. A. S., KUNTAEGOWDANAHALLI, S. S. & PAPAUTSKY, I. 2008 Continuous particle separation in spiral microchannels using dean flows and differential migration. *Lab. Chip* **8** (11), 1906–1914.
- CHERUKAT, P. & MCLAUGHLIN, J. B. 1994 The inertial lift on a rigid sphere in a linear shear flow field near a flat wall. *J. Fluid Mech.* **263**, 1–18.
- CHUN, B. & LADD, A. J. C. 2006 Inertial migration of neutrally buoyant particles in a square duct: An investigation of multiple equilibrium positions. *Phys. Fluids* **18**, 031704.
- COX, R. G. & HSU, S. K. 1977 The lateral migration of solid particles in a laminar flow near a plane. *Int. J. Multiph. Flow* **3**, 201–222.
- DI CARLO, D., EDD, J. F. & ET AL. 2009 Particle segregation and dynamics in confined flows. *Phys. Rev. Lett.* **102** (9), 094503.
- DI CARLO, D., IRIMIA, D., TOMPKINS, R. G. & TONER, M. 2007 Continuous inertial focusing, ordering, and separation of particles in microchannels. *Proc. Natl. Acad. Sci. U.S.A.* **104** (48), 18892–18897.
- DUBOV, A. L., SCHMIESCHEK, S., ASMOLOV, E. S., HARTING, J. & VINOGRADOVA, O. I. 2014 Lattice-Boltzmann simulations of the drag force on a sphere approaching a superhydrophobic striped plane. *J. Chem. Phys.* **140** (3), 034707.
- DUTZ, S., HAYDEN, M. E. & HÄFELI, U. O. 2017 Fractionation of magnetic microspheres in a microfluidic spiral: Interplay between magnetic and hydrodynamic forces. *PLOS ONE* **12** (1), e0169919.
- FEUILLEBOIS, F. 2004 Perturbation problems at low Reynolds number. *Lecture Notes-AMAS*.
- GOLDMAN, A. J., COX, R. G. & BRENNER, H. 1967 Slow viscous motion of a sphere parallel to a plane wall - II Couette flow. *Chem. Eng. Sci.* **22**, 653–660.
- HARTING, J., FRUITERS, S., RAMAIOLI, M., ROBINSON, M., WOLF, D. E. & LUDING, S. 2014 Recent advances in the simulation of particle-laden flows. *Eur. Phys. J. Spec. Topics* **223**, 2253–2267.
- HO, B. P. & LEAL, L. G. 1974 Inertial migration of rigid spheres in two-dimensional unidirectional flows. *J. Fluid Mech.* **65**, 365–400.
- HOOD, K., KAHKESHANI, S., DI CARLO, D. & ROPER, M. 2016 Direct measurement of particle inertial migration in rectangular microchannels. *Lab. Chip* **16**, 2840–2850.

- HOOD, K., LEE, S. & ROPER, M. 2015 Inertial migration of a rigid sphere in three-dimensional Poiseuille flow. *J. Fluid Mech.* **765**, 452–479.
- JANOSCHEK, F., TOSCHI, F. & HARTING, J. 2010 Simplified particulate model for coarse-grained hemodynamics simulations. *Phys. Rev. E* **82**, 056710.
- KILIMNIK, A., MAO, W. & ALEXEEV, A. 2011 Inertial migration of deformable capsules in channel flow. *Phys. of Fluids* **23** (12), 123302.
- KRISHNAN, G. P. & LEIGHTON JR., D. T. 1995 Inertial lift on a moving sphere in contact with a plane wall in a shear flow. *Phys. Fluids* **7** (11), 2538–2545.
- KRÜGER, T., KAOUI, B. & HARTING, J. 2014 Interplay of inertia and deformability on rheological properties of a suspension of capsules. *The Journal of Fluid Mechanics* **751**, 725–745.
- KUNERT, C., HARTING, J. & VINOGRADOVA, O. I. 2010 Random-roughness hydrodynamic boundary conditions. *Phys. Rev. Lett.* **105** (1), 016001.
- LADD, A. J. C. & VERBERG, R. 2001 Lattice-Boltzmann simulations of particle-fluid suspensions. *J. Stat. Phys.* **104** (5), 1191.
- LIU, C., HU, G., JIANG, X. & SUN, J. 2015 Inertial focusing of spherical particles in rectangular microchannels over a wide range of Reynolds numbers. *Lab. Chip* **15** (4), 1168–1177.
- LIU, C., XUE, C., SUN, J. & HU, G. 2016 A generalized formula for inertial lift on a sphere in microchannels. *Lab. Chip* **16** (5), 884–892.
- LOISEL, V., ABBAS, M., MASBERNAT, O. & CLIMENT, E. 2015 Inertia-driven particle migration and mixing in a wall-bounded laminar suspension flow. *Phys. Fluids* **27** (12), 123304.
- MARTEL, J. M. & TONER, M. 2014 Inertial focusing in microfluidics. *Annu. Rev. Biomed. Eng.* **16**, 371–396.
- MATAS, J.-P., MORRIS, J. F. & GUAZZELLI, E. 2004 Inertial migration of rigid spherical particles in Poiseuille flow. *J. Fluid Mech.* **515**, 171–195.
- MATAS, J.-P., MORRIS, J. F. & GUAZZELLI, E. 2009 Lateral force on a rigid sphere in large-inertia laminar pipe flow. *J. Fluid Mech.* **621**, 59–67.
- MIURA, K., ITANO, T. & SUGIHARA-SEKI, M. 2014 Inertial migration of neutrally buoyant spheres in a pressure-driven flow through square channels. *J. Fluid Mech.* **749**, 320–330.
- MORITA, Y., ITANO, T. & SUGIHARA-SEKI, M. 2017 Equilibrium radial positions of neutrally buoyant spherical particles over the circular cross-section in Poiseuille flow. *J. Fluid Mech.* **813**, 750–767.
- PASOL, L., SELIER, A. & FEUILLEBOIS, F. 2006 A sphere in a second degree polynomial creeping flow parallel to a wall. *QJ Mech. Appl. Math.* **59** (4), 587–614.
- RESCHIGLIAN, P., MELUCCI, D., TORSI, G. & ZATTONI, A. 2000 Standardless method for quantitative particle-size distribution studies by gravitational field-flow fractionation. application to silica particles. *Chromatographia* **51** (1-2), 87–94.
- SCHONBERG, J. A. & HINCH, E. J. 1989 Inertial migration of a sphere in Poiseuille flow. *J. Fluid Mech.* **203**, 517–524.
- SEGRÉ, G. & SILBERBERG, A. 1962 Behaviour of macroscopic rigid spheres in Poiseuille flow. Part 2. Experimental results and interpretation. *J. Fluid Mech.* **14**, 136–157.
- VASSEUR, P. & COX, R. G. 1976 The lateral migration of a spherical particle in two-dimensional shear flows. *J. Fluid Mech.* **78**, 385–413.
- WAKIYA, S., DARABANER, C.L. & MASON, S.G. 1967 Particle motions in sheared suspensions XXI: Interactions of rigid spheres (theoretical). *Rheol. Acta* **6** (3), 264–273.
- YAHIAOUI, S. & FEUILLEBOIS, F. 2010 Lift on a sphere moving near a wall in a parabolic flow. *J. Fluid Mech.* **662**, 447–474.
- ZHANG, J., YAN, S., ALICI, G., NGUYEN, N.-T., DI CARLO, D. & LI, W. 2014 Real-time control of inertial focusing in microfluidics using dielectrophoresis (dep). *RSC Adv.* **4** (107), 62076–62085.
- ZHANG, J., YAN, S., YUAN, D., ALICI, G., NGUYEN, N.-T., WARKIANI, M. E. & LI, W. 2016 Fundamentals and applications of inertial microfluidics: a review. *Lab. Chip* **16** (1), 10–34.